

Journal of Materials Chemistry A

Accepted Manuscript



This is an *Accepted Manuscript*, which has been through the Royal Society of Chemistry peer review process and has been accepted for publication.

Accepted Manuscripts are published online shortly after acceptance, before technical editing, formatting and proof reading. Using this free service, authors can make their results available to the community, in citable form, before we publish the edited article. We will replace this *Accepted Manuscript* with the edited and formatted *Advance Article* as soon as it is available.

You can find more information about *Accepted Manuscripts* in the [Information for Authors](#).

Please note that technical editing may introduce minor changes to the text and/or graphics, which may alter content. The journal's standard [Terms & Conditions](#) and the [Ethical guidelines](#) still apply. In no event shall the Royal Society of Chemistry be held responsible for any errors or omissions in this *Accepted Manuscript* or any consequences arising from the use of any information it contains.

Growth Control of Compact $\text{CH}_3\text{NH}_3\text{PbI}_3$ Thin Films *via* Enhanced Solid-State Precursor Reaction for Efficient Planar Perovskite Solar Cells†

Yuanyuan Zhou,^a Mengjin Yang,^b Alexander L. Vasiliev,^{a,§} Hector F. Garces,^a Yixin Zhao,^c Dong Wang,^d Shuping Pang,^d Kai Zhu^{b,*} and Nitin P. Padture^{a,*}

^a School of Engineering, Brown University, Providence, RI 02912, USA.

Email: nitin_padture@brown.edu

^b Chemical and Materials Science Center, National Renewable Energy Laboratory, Golden, CO 80401, USA. Email: kai.zhu@nrel.gov

^c School of Environmental Science and Engineering, Shanghai Jiao Tong University, Shanghai 200240, P.R. China

^d Qingdao Institute of Bioenergy and Bioprocess Technology, Chinese Academy of Sciences, Qingdao 266101, P.R. China

Journal of Materials Chemistry A (Paper)
Manuscript TA-ART-12-2014-007036

[§] On leave from National Research Centre “Kurchatov Institute,” Moscow 123182, Russia.

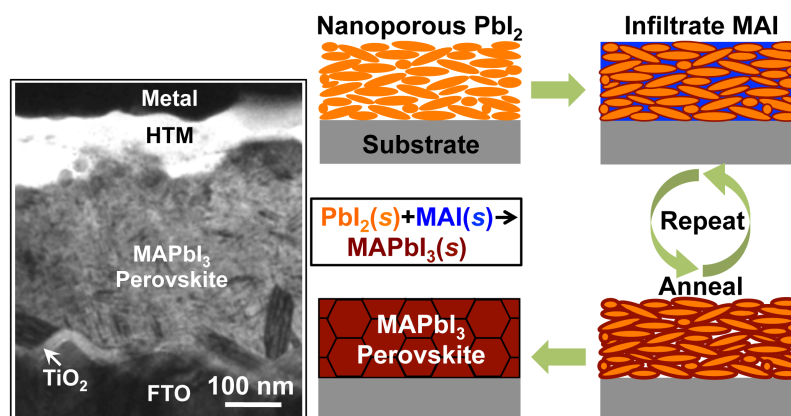
† Electronic Supplementary Information (ESI) available. See doi: 10.1039/c4ta.....

Abstract

$\text{CH}_3\text{NH}_3\text{PbI}_3$ (MAPbI_3) perovskite thin films that are solution-processed using the one-step or the two-step conventional method typically contain significant amount of defects (voids, pinholes) or PbI_2 impurities, which have a detrimental effect on the performance of planar perovskite solar cells (PSCs) fabricated using those films. To overcome this issue, we demonstrate that the enhancement of the solid-state reaction between inorganic-organic precursors is an effective route for the growth of compact, phase-pure MAPbI_3 perovskite thin films with no voids or pinholes. To ensure uniform solid-state conversion ($\text{MAI}+\text{PbI}_2\rightarrow\text{MAPbI}_3$) across the entire film thickness, a new successive spincoating/annealing (SSCA) process is used, where MAI is repeatedly infiltrated into a nanoporous PbI_2 film, followed by thermal annealing. The mechanisms involved in the SSCA process are elucidated by monitoring the evolution of the phases during the reaction. Owing to these desirable characteristics (high-purity, full-coverage, enhanced smoothness and compactness) of the SSCA MAPbI_3 films, planar PSCs based on these perovskite thin films deliver a maximum power conversion efficiency (PCE) close to 15%. Furthermore, PSCs fabricated using partially converted nanoporous PbI_2 thin films deliver a surprising PCE approaching 10%, suggesting continuous MAPbI_3 phase formation throughout the entire film at each spincoating/annealing process. The advantages gained from enhancing the solid-state precursor reactions allow better control over the growth of the perovskite, making the SSCA process more robust.

Graphical Abstract

A new solution-processing method is demonstrated for the deposition of compact $\text{CH}_3\text{NH}_3\text{PbI}_3$ perovskite thin films for high-efficiency planar solar cells.



Introduction

The recent introduction of methylammonium lead triiodide ($\text{CH}_3\text{NH}_3\text{PbI}_3$ or MAPbI_3) perovskite as a strong light absorber has injected great excitement in the field of thin-film photovoltaics.¹⁻⁴ MAPbI_3 possesses a combination of desirable properties^{3,4}, including favourable direct band gap, large absorption coefficient in the visible spectrum, high carrier mobilities, and long carrier-diffusion lengths for both electrons and holes.^{5,6} Over a short period of five years since perovskite solar cells (PSCs) were first introduced,⁷ their power conversion efficiency (PCE) shot up to 20.1%.⁸ While numerous PSCs studies have shown that the morphology of the MAPbI_3 thin film plays a central role in the PSCs performance,⁹ effective control of that morphology through processing still remains a challenge.¹⁰ Typically, deposition of MAPbI_3 perovskite thin films is accomplished using the one-step or the two-step solution-processing method.^{1,3,4,10} The conventional one-step method entails direct spin-coating of MAPbI_3 solution, followed by annealing at 70-150 °C.⁹⁻¹¹ However, it is generally difficult to control perovskite crystallization and film uniformity at the elevated temperature in this method. In this context, the sequential (two-step) solution-processing method (see Fig. S1A), where spin-coated PbI_2 thin films are reacted with $\text{CH}_3\text{NH}_3\text{I}$ (MAI) solution by dipping, followed by annealing, is gaining popularity over the one-step method.^{4,10} In general, the two-step method offers better control over the perovskite morphology compared with the one-step method. This is particularly true in the case of mesoscopic-oxide scaffold films, where complete $\text{PbI}_2 + \text{MAI} \rightarrow \text{MAPbI}_3$ reaction can take place rapidly due to the nanoscale nature of the PbI_2 within the nanoporous scaffolds.¹² However, in the case of planar thin films, prolonged MAI-solution dipping is needed for the completion of the reaction with solution-deposited PbI_2 (typically dense) across the entire thin film that can be few hundred nanometers in thickness.¹² The prolonged contact of the liquid MAI solution with the as-formed MAPbI_3 perovskite thin film appears to degrade its morphology making it somewhat porous with voids and pinholes (Fig. S1B), which is attributed to partial dissolution of perovskite ($\text{MAPbI}_3 \rightarrow \text{MA}^+ + \text{I}^- + \text{PbI}_2$) and the nature of the reaction between solid PbI_2 and liquid MAI solution.¹³ Such defects may cause reduced optical absorption, and the detrimental contact of the subsequently deposited hole-transporting material (HTM) with the TiO_2 blocking layer below the perovskite thin film.^{3,9} Thus, a dense perovskite thin film is generally desired.

In this context, uniform reaction between solid PbI_2 and solid MAI, instead of liquid MAI solution, is expected to provide better control over the planar MAPbI_3 perovskite thin-film morphology and reduce the occurrence of pinholes and voids. This can be achieved by replacing the dense PbI_2 thin film by a nanoporous solid PbI_2 thin film, and replacing the conventional second step of MAI solution dipping with repeated infiltration of MAI *via* spin-coating and then annealing -- a process we call successive spin-coating/annealing (SSCA).¹⁴ The mechanisms by which dense MAPbI_3 perovskite thin films are formed in the SSCA process are elucidated here. In contrast to the conventional two-step process, the promotion of the solid-state reaction between PbI_2 and MAI in the SSCA process results in high quality, compact MAPbI_3 perovskite thin films, precluding any adverse effect of the liquid MAI solution on the films. Here, the SSCA MAPbI_3 perovskite thin films and the planar PSCs made from these films are also characterized extensively. We show that these PSCs deliver a maximum PCE of 14.6%, with an open circuit voltage (V_{OC}) of 1.05 V, which is attributed to the compact nature of the SSCA MAPbI_3 perovskite thin films.

Experimental

Raw chemicals and precursors preparation

All reagent grade chemicals were obtained commercially from Sigma-Aldrich, St. Louis, MO, unless noted otherwise. MAI was prepared in-house. In a typical procedure, 24 ml of 33 wt% methylamine (CH_3NH_2) solution in anhydrous ethanol was reacted with 10 ml of 57 wt% hydroiodic acid (HI) in water, in 100 ml of ethanol (excess CH_3NH_2) in a dry Ar atmosphere at room temperature. The solvent and the excess CH_3NH_2 were removed using a rotary evaporator, and the resulting MAI powder was harvested.

Successive spin-coating/annealing (SSCA) processing of MAPbI_3 perovskite thin films

First, 0.8 M PbI_2 (Alfa-Aesar, Ward Hill, MA) solution in N,N'-dimethylformamide (DMF) was spin-coated onto different substrates: plain glass, quartz, previously patterned fluorine-doped tin oxide (FTO) coated glass (TEC15, Hartford Glass Co., Hartford City, IN), or the patterned FTO-coated glass with a TiO_2 blocking layer (~15 nm). A smooth, nanoporous PbI_2 thin film was formed, which was then dried at room temperature under blowing air. Second, fresh MAI solution of $10 \text{ mg}\cdot\text{ml}^{-1}$ in anhydrous isopropanol was spin-coated onto the as-prepared PbI_2 layer immediately, and it was then annealed at 150°C for 1 min, which constitutes the first SSCA cycle. This SSCA cycle was then repeated 3-4 times. The excess MAI was washed using isopropanol, and the final thin films were annealed at 150°C for 2 min to obtain a dark-colored perovskite film. The film thickness can be controlled *via* spinning conditions. The spin-coating condition of 4000 rpm, 15 s was used for all thin film deposition, which resulted in 250-300 nm MAPbI_3 perovskite thin films. The nature of the substrate (plain glass, quartz, FTO-coated glass, FTO-coated glass with TiO_2 blocking layer) did not have any obvious effects on the SSCA-processed MAPbI_3 perovskite films.

Fabrication of perovskite solar cells

For the fabrication of the PSCs, FTO-coated glass was patterned by 25% hydrochloric acid etching with zinc powder, and cleaned by soaking in a base bath (5 wt % NaOH in ethanol) overnight. After washing using deionized water and ethanol, a compact TiO_2 blocking layer was deposited on top of patterned FTO by spray pyrolysis at 450°C . The perovskite layer was then deposited using the SSCA process (one, two or three SSCA cycles) as described above. This was followed by spin-coating a solution of a HTM, which consisted of 80 mg 2,2',7,7'-tetrakis(N,N-dip-methoxyphenylamine)-9,9'-spirobifluorene (Spiro-MeOTAD; Merck, Germany), 30 μl bis(trifluoromethane) sulfonimide lithium salt stock solution (500 mg Li-TFSI in 1 ml acetonitrile), and 30 μl 4-tert-butylpyridine (TBP), and 1 ml chlorobenzene solvent. The HTM spin-coating process was performed in a dry-air atmosphere with humidity below 10%. Finally a 150 nm Ag layer was deposited using thermal evaporator and a shadow mask. The PSCs were stored in a dry-air atmosphere with humidity below 5%, and typically the performance of the PSC was measured one day after their fabrication.

Film and device structure characterization

X-ray diffraction (XRD) was performed on a X-ray diffractometer (D8-Advance, Bruker, Germany) using $\text{Cu K}\alpha_1$ radiation ($\lambda=1.5406 \text{ \AA}$) at step size/time $0.02^\circ/1 \text{ s}$ conditions. Surface morphology of the films were observed in a scanning electron microscope (SEM; LEO 1530VP, Carl Zeiss, Germany). The local roughness of the MAPbI_3 thin films were characterized using an atomic force microscope (AFM; 5500, Agilent, Santa Clara, CA) operated in contact mode.

Optical spectroscopy (transmission, reflection, absorption) of the films on quartz at each formation stage was conducted on a spectral response measurement system (QEXL, PV Measurements, Boulder, CO). Transmission electron microscopy (TEM) was used to characterize cross-sections of the whole PSCs. Note that this particular PSC has a thinner HTM layer compared to most of the other PSCs fabricated in this study. Samples from specific locations on the cross-sections were prepared by focused ion beam (FIB; Helios 600, FEI, Hillsboro, OR) and *in situ* lift-out. The TEM specimens were examined using TEM (2100F, JEOL, Tokyo, Japan) operated at 200 kV accelerating voltage.

Performance characterization of perovskite solar cells

The incident external quantum efficiency (EQE) spectra of the PSCs were recorded at a chopping frequency of 5 Hz in AC mode on a solar cell quantum efficiency measurement system (QEX10, PV Measurements, Boulder, CO). The current density (J) - voltage (V) characteristics of the PSCs were obtained using a 2400 SourceMeter (Keithley, Cleveland, OH) under simulated one-sun AM 1.5G illumination ($100 \text{ mW}\cdot\text{cm}^{-2}$) (Oriel Sol3A Class AAA Solar Simulator, Newport Corporation, Irvine, CA). A typical J - V scan starts from forward-bias to short-circuit at the rate of $20 \text{ mV}\cdot\text{s}^{-1}$. A typical active area of 0.12 cm^2 was defined using a non-reflective mask for the J - V measurements. The steady-state maximum power output of the solar cells was measured by monitoring the current density (J) output at the maximum power voltage (V) bias for up to 300 s using a VersaSTAT MC potentiostat (Princeton Applied Research, Acton, MA). The current output can be converted to power conversion efficiency (PCE) output using the following relation: $\text{PCE} = (J (\text{mA}\cdot\text{cm}^{-2}) \times V (\text{V})) / (100 (\text{mW}\cdot\text{cm}^{-2}))$. A shutter was used to switch on and off the one-sun illumination on the cell. The solar-cell testing was conducted in ambient atmosphere with humidity of 20-40%. Impedance spectroscopy (IS) on the PSCs was performed using a PARSTAT 2273 workstation (Princeton Applied Research, Acton, MA) with the frequency range of 0.1 Hz–100 kHz and the modulation amplitude of 10 mV. The IS spectra were analyzed using ZView 2.9c software (Scribner Associates, Southern Pines, NC).

Results and Discussion

SSCA process description and deposition mechanisms

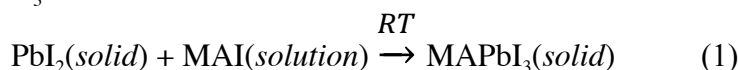
The SSCA process is depicted schematically in Fig. 1. Briefly, a nanoporous PbI_2 thin film is first solution-deposited on a substrate, and MAI is then infiltrated *via* spin-coating. This is followed by thermal annealing, resulting in the rapid formation of the MAPbI_3 perovskite. The MAI infiltration/annealing process is repeated 3-4 times (cycles), which results in the full conversion of the entire PbI_2 thin film into a compact MAPbI_3 perovskite thin film. Note that it is critical to have a nanoporous PbI_2 thin film that allows effective capillary infiltration of the MAI solution.¹⁵ Such nanoporous PbI_2 is produced *via* room-temperature drying (under blowing air) of spin-coated PbI_2 (solution in DMF) films, whereas conventional drying at higher temperatures (70 to 150 °C) results in dense PbI_2 films (see Fig. S2). Figures 2A-2D show a series of XRD patterns following the phase evolution during the SSCA process. The indexed XRD pattern in Fig. 2A from the solution-deposited PbI_2 thin film shows strong $\langle 100 \rangle$ texture, which is consistent with what has been observed by others in PbI_2 thin films derived from solutions in DMF solvent.¹⁶ The XRD patterns in Figs. 2B, 2C, and 2D from the thin films after one, two, and three SSCA cycles, respectively, show the evolution and completion of the $\text{PbI}_2 + \text{MAI} \rightarrow \text{MAPbI}_3$ reaction, with no PbI_2 observed in Fig. 2D. The indexed XRD pattern in

Fig. 2D confirms the presence of pure β -MAPbI₃ phase (space group $I4/mcm$ ^{17,18}). More SSCA cycles result in the undesirable deposition of excess solid MAI on the surface (not shown here).

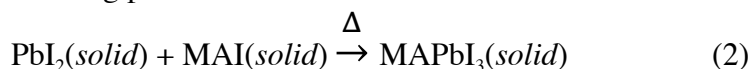
Figures 3A-3D are SEM images of top surfaces of the thin films corresponding to those in Figs. 2A-2D. In Fig. 3A, the PbI₂ crystals appear “plate” like, which is consistent with the strong texture observed in the XRD pattern (Fig. 2A). The PbI₂ thin film also appears nanoporous, and it is presumed that the interconnected pore channels extend through the thickness of the film. As mentioned earlier, such a nanoporous structure in the PbI₂ thin film is necessary for the SSCA process to work. With increasing number of SSCA cycles, the porosity reduces (Figs. 3B to 3D), which is related to the volume expansion associated with the intercalation of MAI into the PbI₂ structure to form MAPbI₃ perovskite.¹⁶ This volume expansion originates from the crystallographic reconstruction of edge-sharing octahedra in PbI₂ (density 6.16 g.cm⁻³) to corner-sharing octahedra in MAPbI₃ perovskite (density 4.16 g.cm⁻³).^{17,18} Also, the crystal shapes become more equiaxed with increased SSCA cycles, indicating a loss of texture. The MAPbI₃ perovskite thin film in Fig. 3D shows complete uniform coverage and compact morphology. The atomic force microscope (AFM) scan in Fig. 3E shows a smooth MAPbI₃ perovskite thin film, with a root mean square (RMS) roughness of 19.5 nm.

Figure 4 presents the evolution of the optical absorption spectra, corresponding to Figs. 3A-3D, during the SSCA process. With increasing number of SSCA cycles, a transition from PbI₂, with its sharp edge at ~520 nm, to pure MAPbI₃ perovskite, with its weak optical bleaching at ~570 nm and strong optical bleaching at ~760 nm,^{5,19} is observed. These optical absorption results are consistent with the XRD (Fig. 2A-2D) and SEM (Fig. 3A-3D) observations.

It is clear from Fig. 3A that the pure PbI₂ thin film is nanoporous. During the first SSCA cycle of spin-coating of MAI solution, but before annealing, MAI infiltrates the PbI₂ nanopores and the following reaction takes place immediately upon contact at room temperature producing some amount of MAPbI₃:



This is confirmed in the XRD pattern of such a thin film in Fig. 5A (without annealing) which shows the presence of MAPbI₃, in addition to PbI₂ and MAI. Also, the SEM image of the top surface of that thin film in Fig. 5B shows traces of unreacted solid MAI, which appears to have crystallized during spin-coating by evaporation of the low-boiling point isopropanol solvent. Subsequent annealing promotes the solid-state reaction:



where all the MAI is consumed (Fig. 3B) and significantly more MAPbI₃ is produced, as observed in the XRD pattern in Fig. 2B. This is also confirmed visually, where the pure PbI₂ thin film darkens as soon MAI is first spin-coated, and darkens further after the annealing step (see Fig. S3). It is likely that the MAPbI₃ forms as a continuous layer on the surfaces of the PbI₂ platelets throughout the film during the first SSCA cycle, and the subsequent SSCA cycles result in the complete transformation of the PbI₂ into MAPbI₃. In this context, a variation of sequential deposition has been reported recently,^{20,21} where inter-diffusion between MAI-PbI₂ stacking layers is claimed as the mechanism for the formation of the perovskite. This mechanism is not likely to be operative in the SSCA method because no distinct MAI layer on top of the spin-coated PbI₂ layer is observed in Fig. 5B. This can be attributed to a more porous PbI₂ film and the relatively low concentration (10 mg.ml⁻¹) of the MAI solution used here in the SSCA process,

compared to what has been used by Xiao *et al.*²⁰ (MAI concentration 17.5-50 mg.ml⁻¹). Thus, in the SSCA process, the perovskite most likely forms by the solid-solid reaction between the interspersed mixture of MAI and PbI₂ throughout the thickness of the thin film.

Solar cells based on SSCA perovskite thin films

Figures 6A-6D are cross-sectional transmission electron microscopy (TEM) bright-field images of the whole PSC fabricated using SSCA (three cycles) MAPbI₃ perovskite thin film. The overall view in Fig. 6A shows the compact nature of the MAPbI₃ thin film (~300 nm) and a well-constructed PSC with all its layers clearly delineated. Note the lack of any infiltration of HTM into the perovskite layer. Figure 6B shows a detailed view of the dense TiO₂ blocking layer (~15 nm), and high crystallinity in the MAPbI₃ layer. In Fig. 6C, well-defined grains and grain boundaries of MAPbI₃ perovskite are observed, and no pores/voids are visible even at the nanoscale. Such highly crystalline, dense structure of the perovskite thin film contributes to efficient light absorption and charge transport. The inset in Fig. 6C shows a high-resolution TEM image with interplanar spacing of ~0.64 nm, corresponding to (110) or (002) planes, further confirming the β -MAPbI₃ phase (lattice parameters: $a=b=8.849$ Å, $c=12.642$ Å¹⁸). Figure 6D is a TEM image of the interface between the MAPbI₃ and the HTM layers showing crystallinity of the MAPbI₃ right up to the interface. Figure 6E is a scanning-TEM image of the whole PSC and energy dispersive spectroscopy (EDS) elemental maps defining the different layers.

The TEM results confirm the formation of fully dense perovskite thin film. Such dense absorber layer eliminates any direct contact between HTM and the TiO₂-blocking layer which can act as a parallel diode in the equivalent circuit of the planar PSCs and decreases the V_{OC} of the corresponding PSCs.⁹ Therefore, a high V_{OC} value of 1.05 V (Table 1) was achieved in these PSCs without the use of any interfacial engineering. For comparison, V_{OC} less than 1 V is generally reported in PSCs employing similar structures made by various other solution-processing methods.^{9,16,22-27} This high V_{OC} value is also comparable to that reported recently for PSCs based on “solvent engineering” of the MAPbI₃ perovskite thin films.^{28,29}

Figure 7A presents typical J - V characteristics of PSCs made with MAPbI₃ perovskite thin films processed using one or three SSCA cycles, under simulated one-sun AM 1.5G (100 mW·cm⁻²) illumination. The solar cell performance parameters extracted from these data are presented in Table 1. The PSC using one SSCA cycle shows an overall PCE of 9.1%, with a short circuit current density (J_{SC}) of 15.8 mA·cm⁻², open circuit voltage (V_{OC}) of 1.04 V, and fill factor (FF) of 0.554. This performance level for a planar PSC is quite remarkable considering the significant amount of PbI₂ present in the perovskite thin film (Fig. 2B). In contrast, a planar PSC based on MAPbI₃ thin film deposited using the conventional two-step method, which also contains significant amount of PbI₂, shows a very low PCE of 0.62% (see Fig. S4). This is attributed to the low J_{sc} value of 1.82 mA·cm⁻². The residual PbI₂ in the conventional two-step process typically exists as a layer between the MAPbI₃ perovskite and the TiO₂ blocking layer. As pointed out in an earlier study, the PbI₂ layer can act as a barrier for electron transfer from perovskite into TiO₂.³⁰ In contrast, the residual PbI₂ in the SSCA approach (one cycle) most likely exists as a distributed second phase throughout the perovskite film, and it does not affect the charge extraction significantly, as indicated by the reasonably high J_{SC} value of 15.8 mA·cm⁻². This makes the SSCA a robust solution-processing method for depositing MAPbI₃ perovskite thin films. While the performance of the one-SSCA-cycle PSC is reasonable, a significant improvement in the J_{SC} by ~23% (19.5 mA·cm⁻²) is observed in a typical three-SSCA-cycles PSC, reaching a PCE of 12.8%. The improved J_{sc} value for these PSCs is consistent with the

enhanced absorption (Fig. 4) associated with the complete conversion of PbI_2 to MAPbI_3 (Fig. 2). (Fifteen each of one- and three-SSCA-cycle PSCs were tested; the maximum, minimum, and average PCE values are reported in Fig. S5.)

According to a procedure suggested by Snaith *et al.*³¹, the stability of the maximum-power-point PCE of both PSCs as a function of time is measured, as shown in Fig. 7B. The steady-state PCEs of the one-SSCA-cycle and the three-SSCA-cycles PSCs reach $\sim 9\%$ and $\sim 12\%$, respectively, consistent with the PCE from the J - V characteristics (Fig. 7A and Table 1). However, the steady-state PCE of the one-SSCA-cycle PSC degrades down to $\sim 7\%$, which could be due to the defects present in the perovskite thin film, whereas the PCE of the three-SSCA-cycles PSC exhibits promising stability over time.

Recombination resistance values (R_{Recomb}) as a function of bias voltage (V) for one-SSCA and three-SSCA cycle PSCs are presented in Fig. 7C. These are calculated from the analysis of the impedance measurements (see Fig. S6) using a model described elsewhere.^{32,33} While the impedances of the two cells are similar, they diverge slightly at higher bias voltages. These results, and the reasonably high PCEs and J_{sc} values observed in one-SSCA-cycle PSC in Fig. 7A, suggest that there are no significant changes in the junction properties at the TiO_2 /perovskite and/or perovskite/HTM interfaces after the first SSCA cycle.³³ This is consistent with the discussion above, where the MAPbI_3 forms as a continuous layer on the PbI_2 platelets by reactions (1) and (2) throughout the thin film.

Fig. 8A presents the J - V characteristics of the best PSC based on SSCA MAPbI_3 perovskite thin film. The PCE is as high as 14.6%, and reaches a level obtained in PSCs based on MAPbI_3 perovskite thin films made by vapour deposition and solution-vapour hybrid deposition.^{16,34-37} For this PSC (Fig. 8A), the J_{sc} is $20.1 \text{ mA}\cdot\text{cm}^{-2}$, V_{oc} is 1.05 V, and FF is 0.692. The integrated J_{sc} value of $19.1 \text{ mA}\cdot\text{cm}^{-2}$ from the EQE- λ spectrum in Fig. 8B is consistent with the corresponding values from the J - V characteristics. These excellent photovoltaic parameters are attributed to the enhanced light-harvesting and charge-transporting properties in the SSCA MAPbI_3 perovskite films with superior phase purity, compactness, smoothness, and full-coverage.^{9,38} The SSCA method, and the idea of promoting solid-state precursor reaction, presented here have generic appeal, and the SSCA method could be extended to other hybrid-perovskite materials and/or other PSC configurations.

Conclusions

We have demonstrated the effectiveness of promoting solid-state reaction between organic-inorganic precursors *via* a new SSCA process in the controlled formation of MAPbI_3 perovskite thin films. Results from characterization studies indicate that multiple SSCA cycles result in complete solid-state reaction between PbI_2 and MAI, resulting in phase-pure, compact, and smooth perovskite thin films with full coverage. Properties of the planar PSCs fabricated using the SSCA-processed MAPbI_3 perovskite thin films lend further support for the proposed deposition mechanisms. While PSCs fabricated from fully-reacted SSCA MAPbI_3 perovskite thin films deliver a maximum PCE close to 15%, PSCs with partially-reacted thin films deliver a PCE approaching 10%, attesting to the robustness of the SSCA method. Thus, SSCA constitutes a new, robust solution-processing route for controlled-morphology deposition of high quality hybrid perovskites for next-generation solar cells.

Acknowledgements

This work was supported by a grant from the National Science Foundation (Grant No. DMR-1305913) and the Brown University Graduate School, and the work at the National Renewable Energy Laboratory was supported by the U.S. Department of Energy under Contract No. DE-AC36-08-GO28308. M.Y. and K.Z. acknowledge the support by the U.S. Department of Energy (DOE) SunShot Initiative under the Next Generation Photovoltaics 3 program (DE-FOA-0000990). We thank Prof. S. Kim, Mr. P. Liu, Prof. D. Pacifici, and Mr. M. Strauss of Brown University for experimental assistance and fruitful discussions.

Notes and references

- 1 H. J. Snaith, *J. Phys. Chem. Lett.*, 2013, **4**, 3623-3630.
- 2 M. He, D. Zheng, M. Wang, C. Lin, and Z. Lin, *J. Mater. Chem. A*, 2014, **2**, 5994-6003.
- 3 M. Grätzel, *Nature Mater.*, 2014, **13**, 838-842.
- 4 H. S. Jung and N.-G. Park, *Small*, 2015, **11**, 10-25.
- 5 G. Xing, N. Mathews, S. Sun, S. S. Lim, Y. M. Lam, M. Grätzel, S. Mhaisalkar and T. C. Sum, *Science*, 2013, **342**, 344-347.
- 6 S. D. Stranks, G. E. Eperon, G. Grancini, C. Menelaou, M. J. P. Alcocer, T. Leijtens, L. M. Herz, A. Petrozza and H. J. Snaith, *Science*, 2013, **342**, 341-344.
- 7 A. Kojima, K. Teshima, Y. Shirai and T. Miyasaka, *J. Am. Chem. Soc.*, 2009, **131**, 6050-6051.
- 8 http://www.nrel.gov/ncpv/images/efficiency_chart.jpg (accessed January 15, 2015).
- 9 G. E. Eperon, V. M. Burlakov, P. Docampo, A. Goriely and H. J. Snaith, *Adv. Funct. Mater.*, 2014, **24**, 151-157.
- 10 Y. Zhao and K. Zhu, *J. Phys. Chem. Lett.*, 2014, **5**, 4175-4186.
- 11 H. Zhou, Q. Chen, G. Li, S. Luo, T.-B. Song, H.-S. Duan, Z. Hong, J. You and Y. Yang, *Science*, 2014, **345**, 542-546.
- 12 J. Burschka, N. Pellet, S.-J. Moon, R. Humphrey-Baker, P. Gao, M. K. Nazeeruddin and M. Grätzel, *Nature*, 2013, **499**, 316-319.
- 13 J. Yi and G. Chumanov, *Chem. Lett.*, 2014, **43**, 1722-1731.
- 14 Y. Kutes, L. Ye, Y. Zhou, S. Pang, B. D. Huey and N. P. Padture, *J. Phys. Chem. Lett.*, 2014, **5**, 3335-3339.
- 15 D. I. Dimitrov, A. Milchev and K. Binder, *Phys. Rev. Lett.*, 2007, **99**, 054501.
- 16 Q. Chen, H. Zhou, Z. Hong, S. Luo, H.-S. Duan, H.-H. Wang, Y. Liu, G. Li and Y. Yang, *J. Am. Chem. Soc.*, 2014, **136**, 622-625.
- 17 T. Baikie, Y. Fang, J. M. Kadro, M. Schreyer, F. Wei, S. G. Mhaisalkar, M. Grätzel and T. J. White, *J. Mater. Chem. A*, 2013, **1**, 5628-5641.
- 18 C. C. Stoumpos, C. D. Malliakas and M. G. Kanatzidis, *Inorganic Chemistry*, 2013, **52**, 9019-9038.
- 19 H. Hu, D. Wang, Y. Zhou, J. Zhang, S. Lv, S. Pang, X. Chen, Z. Liu, N. P. Padture, G. Cui, *RSC Adv.*, 2014, **4**, 28964-28967.
- 20 Z. Xiao, C. Bi, Y. Shao, Q. Dong, Y. Yuan, C. Wang, Y. Gao and J. Huang, *Energy Environ. Sci.*, 2014, **7**, 2619-2623.
- 21 C. Bi, Y. Shao, Y. Yuan, Z. Xiao, C. Wang, Y. Gao and J. Huang, *J. Mater. Chem. A*, 2014, **2**, 18508-18514.
- 22 A. T. Barrows, A. J. Pearson, C. K. Kwak, A. D. F. Dunbar, A. R. Buckley and D. G. Lidzey, *Energy Environ. Sci.*, 2014, **7**, 2944-2950.

- 23 M. Jiang, J. Wu, F. Lan, Q. Tao, D. Gao and G. Li, *J. Mater. Chem. A*, 2015, **3**, 963-967.
- 24 Y.-J. Jeon, S. Lee, R. Kang, J.-E. Kim, J.-S. Yeo, S.-H. Lee, S.-S. Kim, J.-M. Yun and D.-Y. Kim, *Sci. Rep.*, 2014, **4**, 6953.
- 25 X. Cui, K. Jiang, J.-H. Huang, X. Zhou, M. Su, S.-G. Li, Q.-Q. Zhang, L.-M. Yang and Y. Song, *Chem. Comm.*, 2015, **51**, 1457-1460.
- 26 D. Shen, X. Yu, X. Cai, M. Peng, Y. Ma, X. Su, L. Xiao and D. Zou, *J. Mater. Chem. A*, 2014, **2**, 20454-20461.
- 27 P. Docampo, F. C. Hanusch, S. D. Stranks, M. Doblinger, J. M. Feck, M. Ehrensperger, N. K. Minar, M. B. Johnston, H. J. Snaith and T. Bein, *Adv. Energy Mater.*, 2014, **4**, 1400355.
- 28 N. J. Jeon, J. H. Noh, Y. C. Kim, W. S. Yang, S. Ryu and S. I. Seok, *Nat. Mater.*, 2014, **9**, 897-903.
- 29 M. Xiao, F. Huang, W. Huang, Y. Dkhissi, Y. Zhu, J. Etheridge, A. Gray-Weale, U. Bach, Y.-B. Cheng and L. Spiccia, *Angew. Chem. Intl. Ed.*, 2014, **53**, 9898-9903.
- 30 Y. Zhao, A. M. Nardes and K. Zhu, *Faraday Discussions*, 2014, doi: 10.1039/C4FD00128A.
- 31 H. J. Snaith, A. Abate, J. M. Ball, G. F. Eperon, T. Leijtens, N. K. Noel, S. D. Stranks, J. T.-W. Wang, K. Wojciechowski and W. Zhang, *J. Phys. Chem. Lett.*, 2014, **5**, 1511-1515.
- 32 Y. Zhao and K. Zhu, *J. Phys. Chem. C*, 2014, **118**, 9412-9418.
- 33 J. A. Christians, R. C. M. Fung and P. V. Kamat, *J. Am. Chem. Soc.*, 2014, **136**, 758-764.
- 34 M. Liu, M. B. Johnston and H. J. Snaith, *Nature*, 2013, **501**, 395-398.
- 35 C.-W. Chen, H.-W. Kang, S. Y. Hsiao, P.-F. Yang, K.-M. Chiang and H.-W. Lin, *Adv. Mater.*, 2014, **26**, 6647-6652.
- 36 L. K. Ono, S. Wang, Y. Kato, S. R. Raga and Y. Qi, *Energy Environ. Sci.*, 2014, **7**, 3989-3993.
- 37 M. R. Leyden, L. K. Ono, S. R. Raga, Y. Kato, S. Wang and Y. Qi, *J. Mater. Chem. A*, 2014, **2**, 18742-18745.
- 38 D. Wang, Z. Liu, Z. Zhou, H. Zhu, Y. Zhou, C. Huang, Z. Wang, H. Xu, Y. Jin, B. Fan, S. Pang and G. Cui, *Chem. Mater.*, 2014, **26**, 7145-7150.

Table 1. Solar cell performance parameters extracted from the *J-V* characteristics in Figs. 7A and 8A.

Number of SSCA Cycles	J_{sc} (mA·cm ⁻²)	<i>FF</i>	V_{oc} (V)	PCE (%)
One	15.8	0.554	1.04	9.1
Three	19.5	0.629	1.04	12.8
Three*	20.1	0.692	1.05	14.6

* Best PSC

Figures Captions

Figure 1. Schematic illustration of the successive spin-coating/annealing (SSCA) solution-processing method for the deposition of MAPbI₃ perovskite thin films.

Figure 2. XRD patterns from thin film on plain glass substrate: (A) after PbI₂ deposition (indexed as cubic PbI₂), (B) after one SSCA cycle, (C) after two SSCA cycles, and (D) after three SSCA cycles (indexed as β -MAPbI₃). The dashed line denotes PbI₂ 001 reflection.

Figure 3. SEM micrographs of top surfaces of thin film on a TiO₂-blocking-layer coated FTO-glass substrate: (A) after PbI₂ deposition, (B) after one SSCA cycle, (C) after two SSCA cycles, and (D) after three SSCA cycles. (E) AFM image of the MAPbI₃ perovskite film corresponding to (D) showing RMS roughness of 19.5 nm.

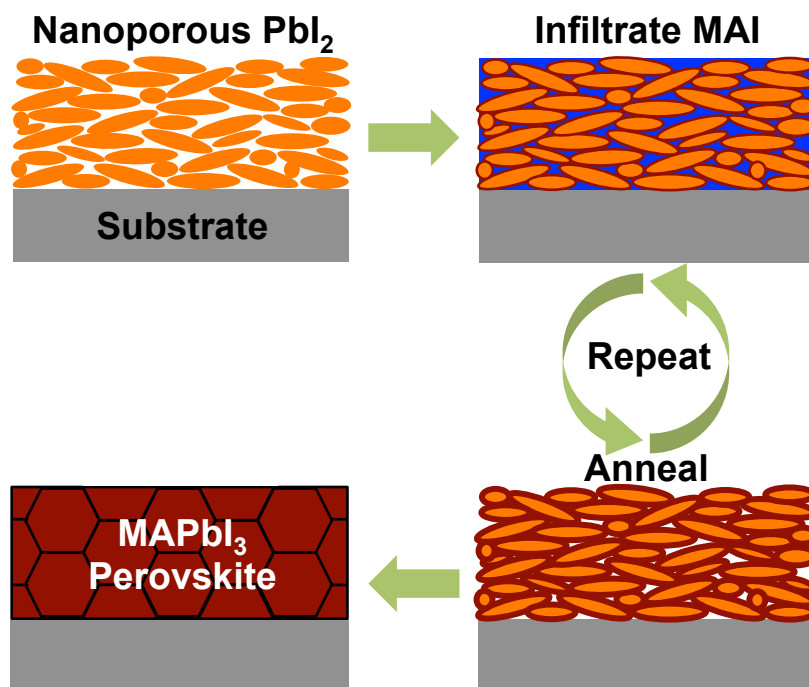
Figure 4. Optical absorption spectra of thin film on a quartz substrate after PbI₂ deposition, and after one, two, and three SSCA cycles.

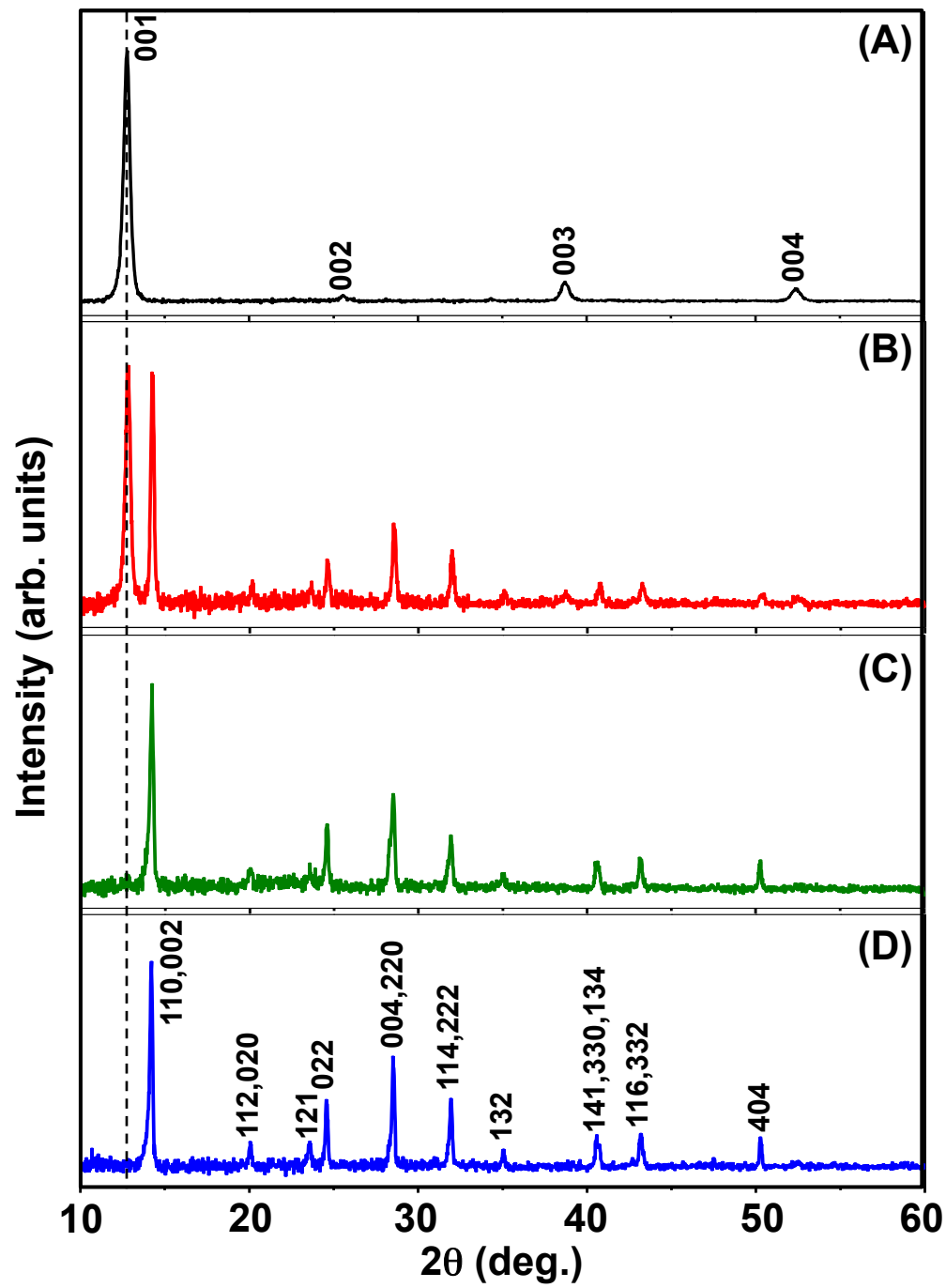
Figure 5. (A) XRD pattern of thin film (on plain glass substrate) after PbI₂ spin-coating followed by MAI spin-coating, but before annealing. The three present phases are marked. (B) SEM image of the top surface of the thin film from (A) showing unreacted MAI (arrows).

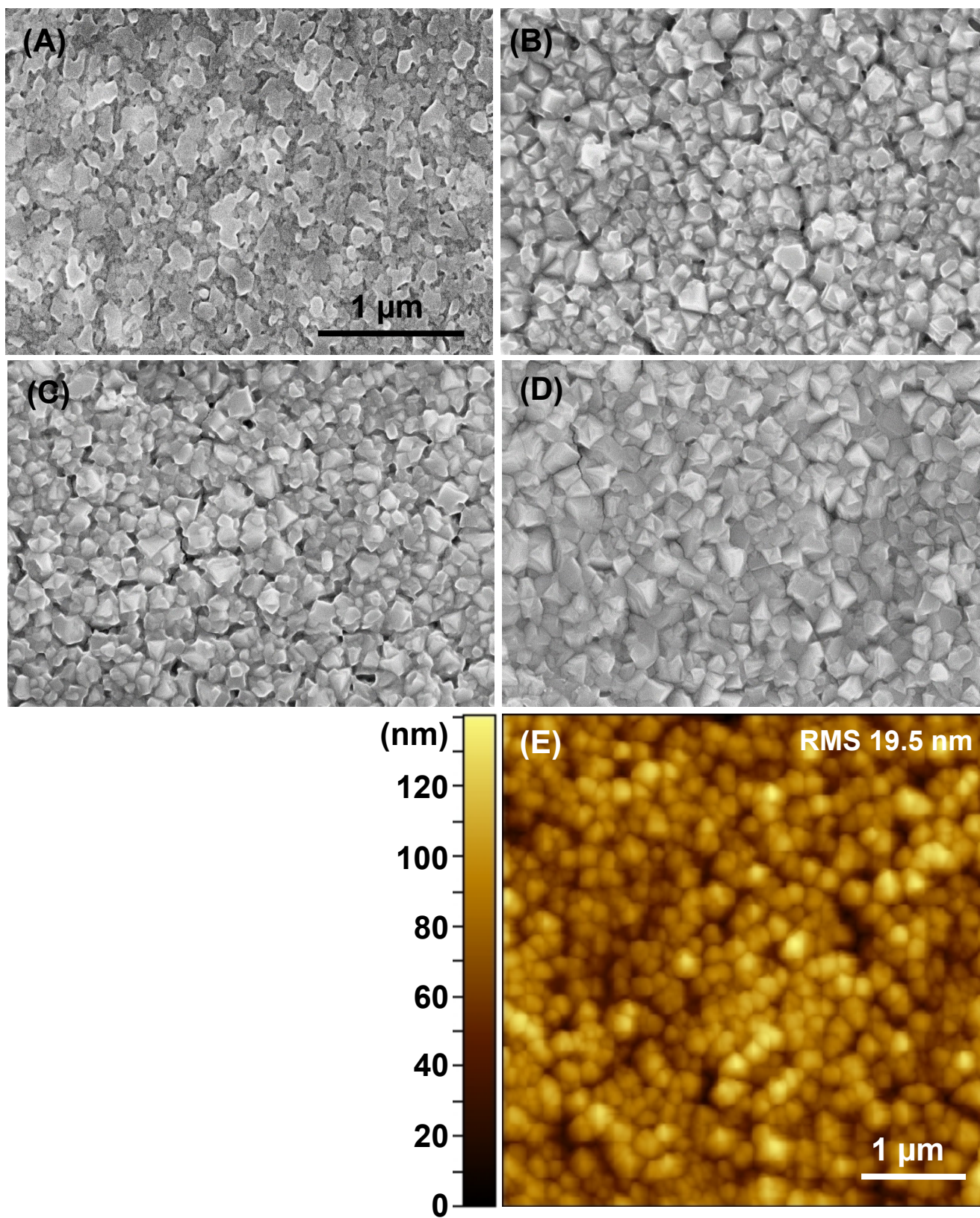
Figure 6. Bright field TEM images of a typical whole PSC, where the MAPbI₃ thin film (~300 nm thickness) is deposited using the SSCA process: (A) overall view, (B) detailed view of interfaces between the FTO, the TiO₂ blocking layer (~15 nm), and the MAPbI₃, (C) detailed view of the polycrystalline MAPbI₃ film (inset: high resolution TEM image showing lattice fringes with interplanar spacing of ~0.64 nm), and (D) detailed view of the interface between the MAPbI₃ and the HTM. (E) STEM image of the whole PSC and corresponding elemental EDS maps showing the distribution of Sn, Ti, Pb, and I.

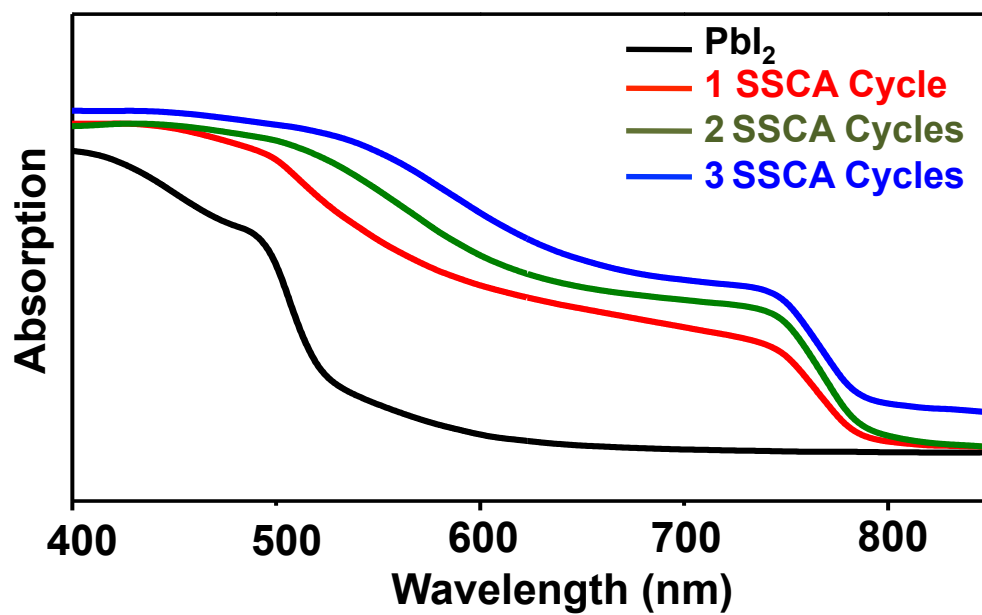
Figure 7. (A) Typical *J-V* characteristics of PSCs based on MAPbI₃ perovskite thin films deposited by the SSCA process (one and three SSCA cycles), under simulated one-sun AM 1.5G (100 mW·cm⁻²) illumination. (B) Steady-state PCE at maximum power as a function of time for a PSC based on MAPbI₃ perovskite thin films deposited by the SSCA process (one and three SSCA cycles). (C) Plots of recombination resistance (R_{Recomb}) as a function of forward bias voltage for PSCs based on MAPbI₃ perovskite thin films deposited by the SSCA process (one and three SSCA cycles).

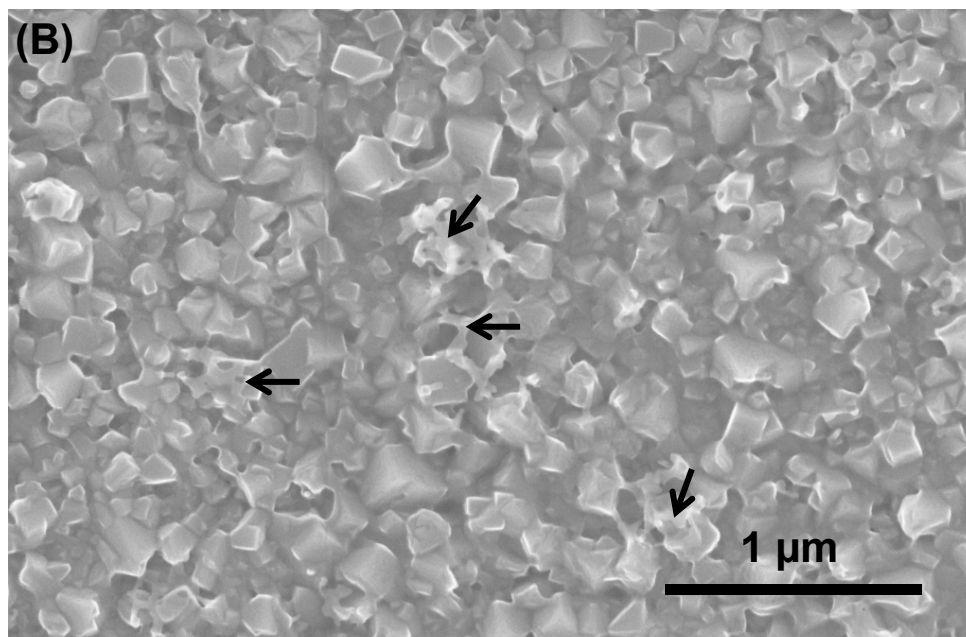
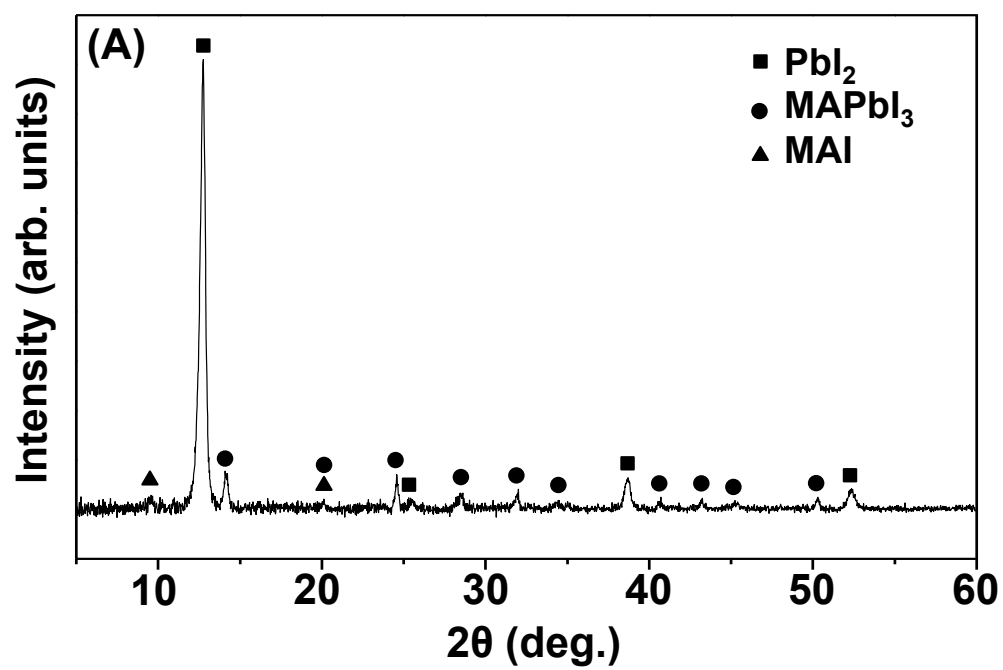
Figure 8. (A) *J-V* characteristics of a 14.6%-efficiency PSC based on MAPbI₃ perovskite thin films deposited by the SSCA process (three SSCA cycles), under simulated one-sun AM 1.5G (100 mW·cm⁻²) illumination. (B) External quantum efficiency (EQE) as a function of wavelength for the PSC in (A).

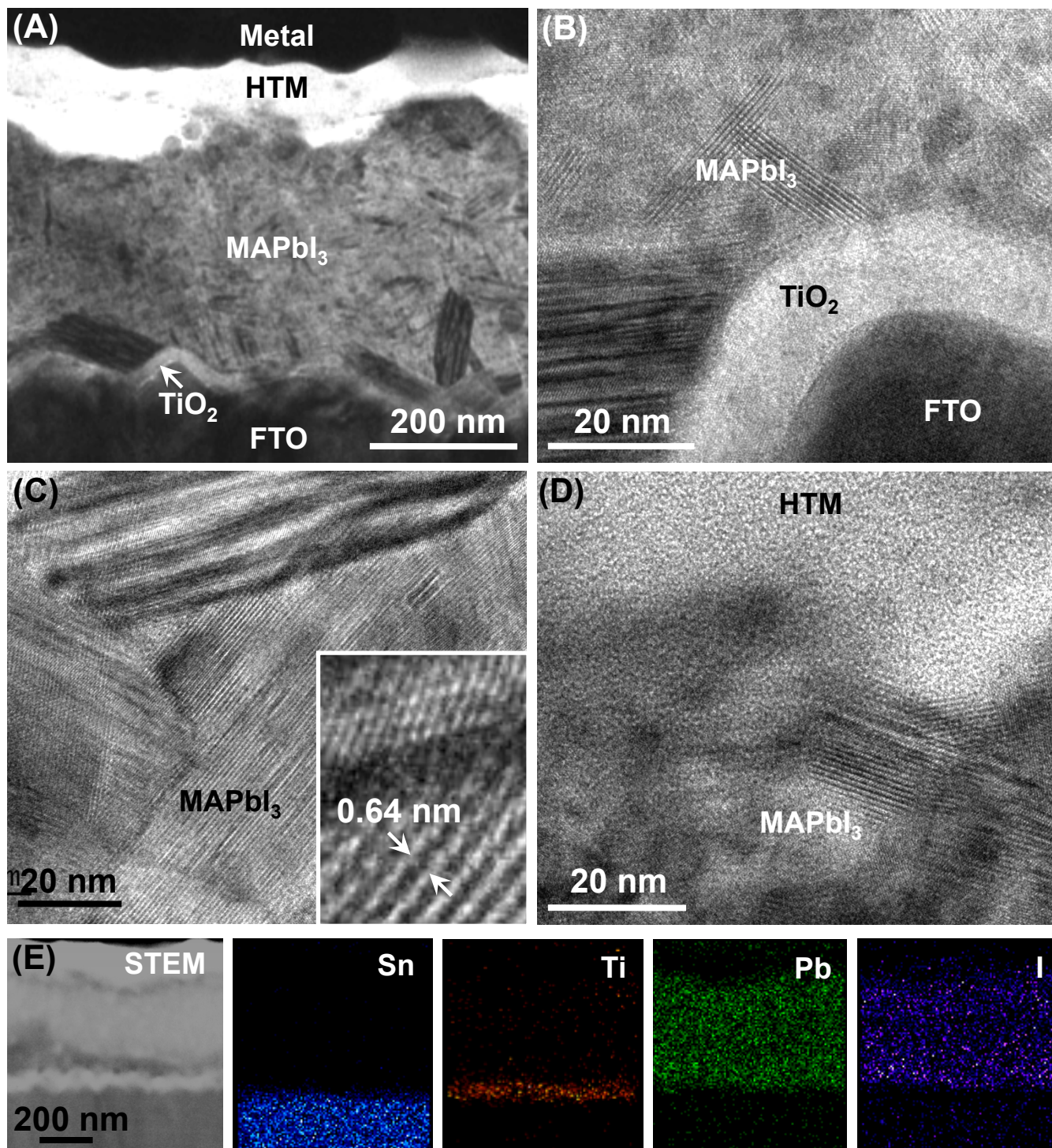


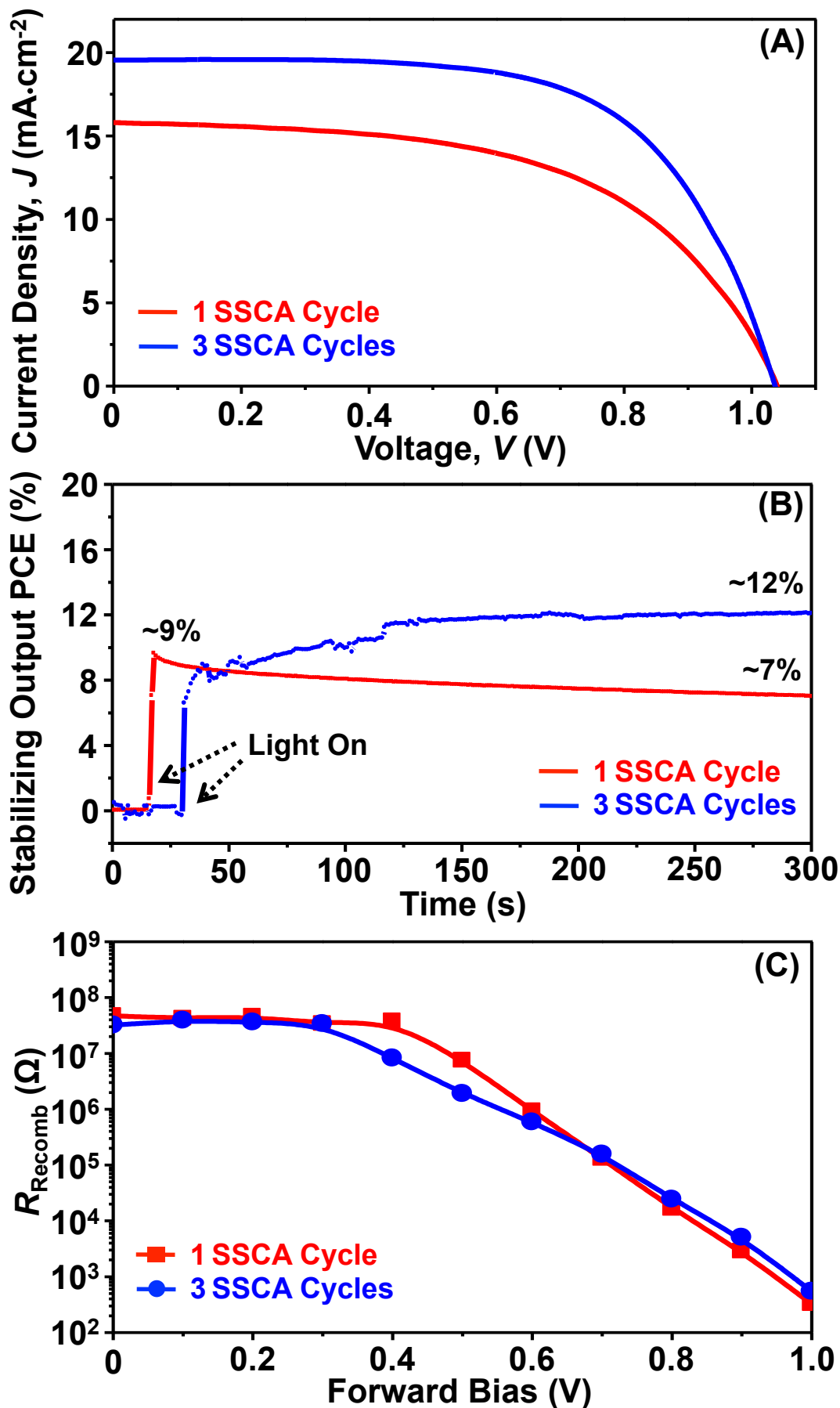
Zhou *et al.*, Figure 2



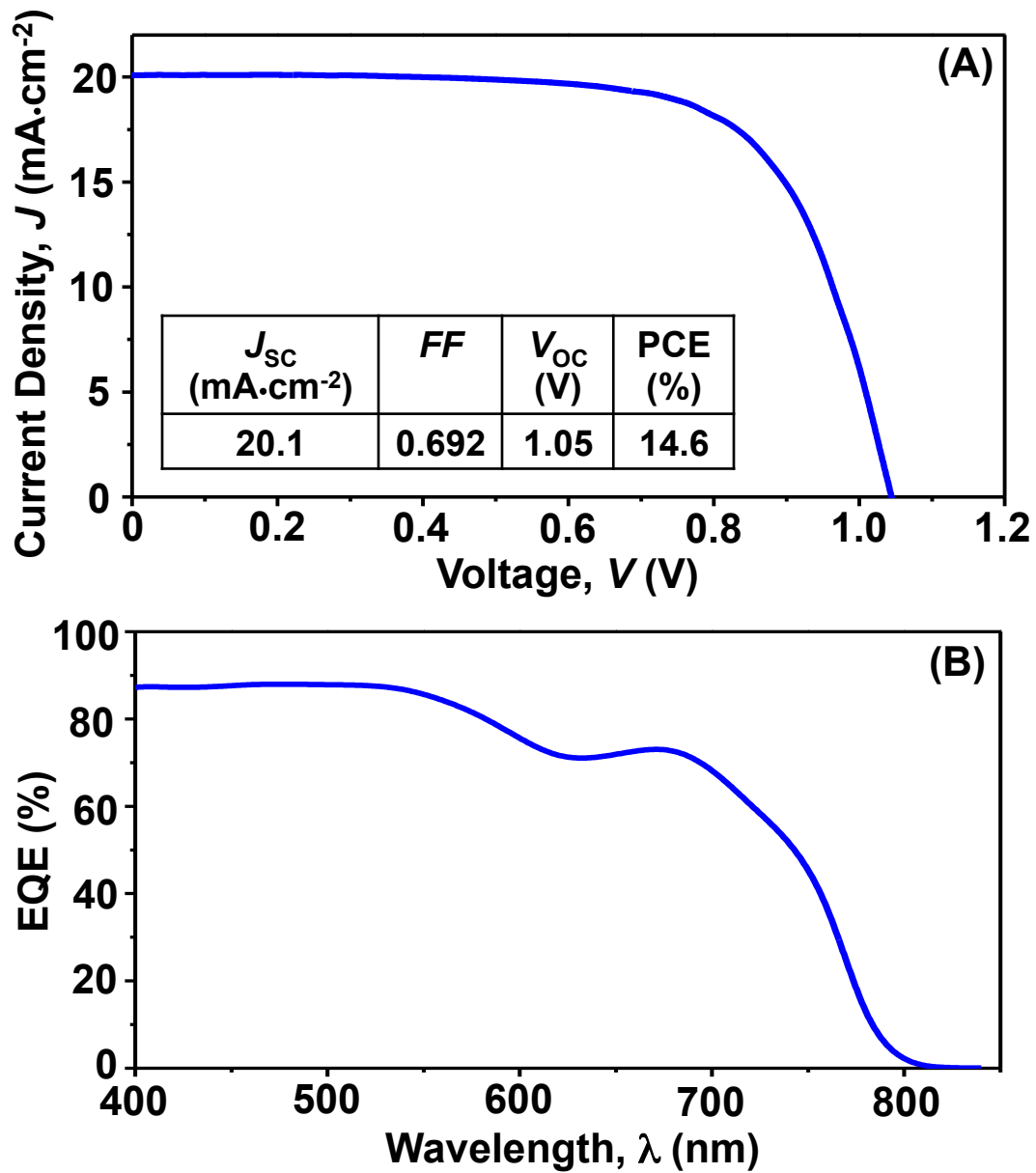








Zhou et al., Figure 7

Zhou *et al.*, Figure 8

Graphical Abstract

A new solution-processing method is demonstrated for the deposition of compact $\text{CH}_3\text{NH}_3\text{PbI}_3$ perovskite thin films for high-efficiency planar solar cells.

